

Changes in ion channel geometry resolved to sub-ångström precision via single molecule mass spectrometry

This article has been downloaded from IOPscience. Please scroll down to see the full text article.

2010 J. Phys.: Condens. Matter 22 454108

(<http://iopscience.iop.org/0953-8984/22/45/454108>)

View [the table of contents for this issue](#), or go to the [journal homepage](#) for more

Download details:

IP Address: 129.6.65.17

The article was downloaded on 01/11/2010 at 11:49

Please note that [terms and conditions apply](#).

Changes in ion channel geometry resolved to sub-ångström precision via single molecule mass spectrometry

Joseph W F Robertson, John J Kasianowicz and Joseph E Reiner

Semiconductor Electronics Division, Electronics and Electrical Engineering Laboratory,
National Institute of Standards and Technology, Gaithersburg, MD 20899, USA

Received 1 April 2010, in final form 1 July 2010

Published 29 October 2010

Online at stacks.iop.org/JPhysCM/22/454108

Abstract

The ion channel formed by *Staphylococcus aureus* alpha-hemolysin switches between multiple open conducting states. We describe a method for precisely estimating the changes in the ion channel geometry that correspond to these different states. Experimentally, we observed that the permeability of a single channel to differently sized poly(ethylene glycol) molecules depends on the magnitude of the open state conductance. A simple theory is proposed for determining changes in channel length of 4.2% and in cross-sectional area of -0.4% .

(Some figures in this article are in colour only in the electronic version)

1. Introduction

The invention of the Coulter counter revolutionized the analysis of blood and other samples containing micron-sized particles [1]. While the device size used in this technology was reduced to hundreds of nanometers in the early 1970s through nuclear track-etched pores in polycarbonate [2], the field languished until biological molecules were discovered to have properties sufficient to extend resistive-pulse sensing down to the molecular scale [3]. Nanopore-based sensing was driven in large part by the hope of rapid, inexpensive DNA sequencing [4] and was extensively reviewed [5–9].

Although pore-based DNA sequencing efforts have garnered the most attention, nanometer-scale pores can also be exploited for chemical analysis. Recently it was shown that the channel formed by *Staphylococcus aureus* α -hemolysin (α HL) could easily determine, with nearly baseline resolution, the polymer number of poly(ethylene glycol) (PEG) in aqueous solution, producing a spectrum analogous to that obtained by traditional mass spectrometry [10]. Here, we expand upon this work to demonstrate that single molecule mass spectrometry can also be used to estimate subtle differences in a nanopore's geometry.

Polymers have been used extensively to probe the properties of ion channels. For example, Zimmerberg and Parsegian demonstrated that PEG and dextran could be used to estimate volumetric changes in the voltage-dependent anion selective channel (VDAC) protein [11]. Specifically, polymers that were too large to enter a VDAC channel caused an osmotic stress on the aqueous solution in the pore, which

shifted the voltage-dependent channel gating equilibrium. The authors concluded that the exodus of water from the pore was accompanied by a concomitant decrease in the pore volume of $\approx 4 \times 10^4 \text{ \AA}^3$. Krasilnikov and colleagues subsequently used polymers to estimate the diameter of ion channels [12–14]. That method took advantage of the ability of pore-permeant nonelectrolyte polymers, which decrease the bulk ionic conductivity, to decrease the pore conductance. The pore diameter was determined from the largest mean polymer molecular mass that decreased the conductance. The latter technique lacked some precision, because the polymers that were used to probe the channel's geometry were polydisperse. The method was recently refined by using the polymer polydispersity information determined with MALDI-TOF mass spectrometry [15]. However, the technique also assumed that all pore-permeant polymers decrease the channel conductance by the same amount, which was recently shown to not be the case [10]. Here, rather than attempting to directly size the nanopore through observing the cutoff size for polymer molecules entering the pore, we use the polydispersity in size of the pore-permeant polymers [10, 16] to estimate very small changes in an ion channel's geometry.

2. Experimental methods and data collection

2.1. Membrane preparation

Solvent-free planar lipid membranes were prepared as follows. DPhyPC (1,2 diphytanoyl-sn-glycero-3-phosphatidylcholine;

Avanti Polar Lipids, Alabaster, AL) bilayers were formed on a glass capillary with a $1.1 \mu\text{m}$ diameter hole prepared as described by White and colleagues [17–19]. The capillary was filled with a mixture of poly(ethylene glycol) (PEG) at $\approx 50 \mu\text{M}$ total PEG content in 4 M KCl (Sigma-Aldrich, St Louis, MO), 10 mM tris (Schwarz/Mann Biotech, Cleveland, OH) at pH 7.2, titrated with saturated citric acid (Fluka, Buchs, Switzerland). The solution external to the capillary was the same 4 M KCl solution, without polymer. Membranes were formed by first treating the glass with $0.4 \mu\text{L}$ of a 0.1% v/v solution of hexadecane in pentane (Sigma-Aldrich). The solution bath external to the glass capillary was coated with $0.6\text{--}1.2 \mu\text{L}$ of DPhyPC dissolved in a 10 mg mL^{-1} mixture in *n*-decane. After ≈ 2 min, the solution level was raised above the pore, spontaneously forming a membrane.

Single channel measurements were obtained by first injecting $0.4\text{--}0.6 \mu\text{L}$ of a 0.5 mg mL^{-1} solution of αHL in pH 7.2 buffer (List biological Laboratories, Campbell, CA) into the bath and applying a slight back pressure (≈ 80 mm Hg to 110 mm Hg) from the capillary side to thin the membrane. After a single channel formed, the pressure was reduced to ≈ 20 mm Hg to prevent further channel insertion and formation.

2.2. Data collection

The experiment monitors the ionic current flowing through a single αHL nanopore with a DC potential (typically -40 mV) applied across the membrane. Polydisperse PEGs with M_w 3000, 2000, 1500 and 1000 g mol^{-1} with an internal standard of chemically purified PEG 1294 g mol^{-1} ($n = 29$), are depicted schematically in figure 1(a). The current was measured using a custom-built, high-impedance integrating amplifier (Electronic Biosciences, San Diego, CA) with a feedback resistance of $2.04 \text{ G}\Omega$ and capacitance of 298 fF . The current time series were digitized at 1.25 MHz with a PCI-6251ADC (National Instruments, Austin, TX). The signal was filtered with an 8-pole low-pass Bessel filter with a 100 kHz corner frequency and down-sampled to 500 kHz for storage and analysis. Prior to analysis, the time series data was further filtered to a cutoff frequency of 10 kHz . PEG reversibly partitions into and out of the pore causing transient current blockades whose amplitudes and residence times scale with the polymer size, figure 1(b). Although the αHL channel can remain in an open state for relatively long periods [20], it is clear from the data that the open channel conductance shifts between at least two different levels. In fact, figure 2 shows that there are at least three stable open state currents that can clearly be resolved when the current is filtered to 10 kHz (orange) and 1 kHz (blue). An all-points histogram of an extended 120 s segment of the data shows three broad peaks in the open channel state, labeled $O1$, $O2$ and $O3$.

2.3. Analysis of open states and polymer blockades

The ionic current time series records were analyzed off-line with an in-house program written in LabVIEW 8.5 (National Instruments). Each transient current blockade caused by individual PEG molecules in the mixture was

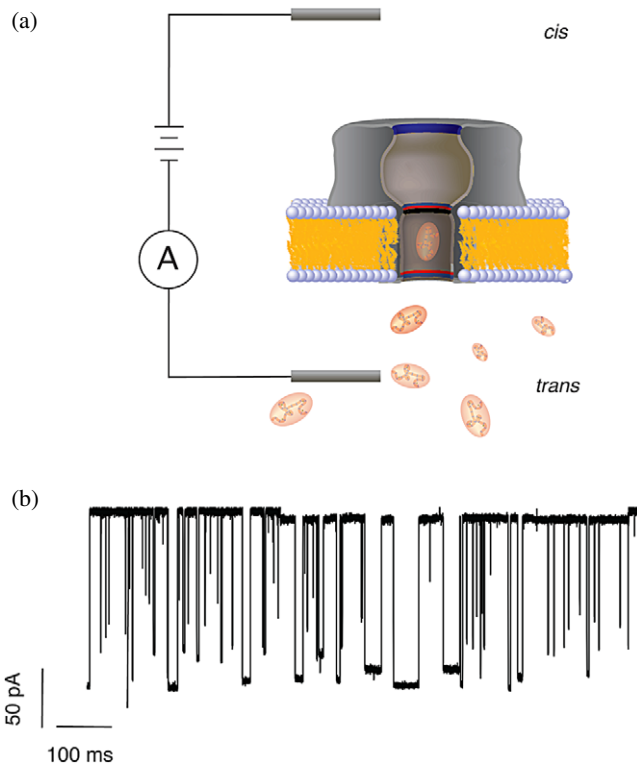


Figure 1. The addition of PEG (ellipsoid particles) to the *trans* side of a single alpha-hemolysin nanopore causes transient current blockades. (a) For the experiments described herein, a bilayer membrane containing a single protein nanopore separates two solution wells of 4 M KCl at pH 7.5. (b) PEG reversibly partitions into and out of the pore causing well-defined blockades.

detected using a threshold and residence time discrimination method. Specifically, current blockades are identified when the magnitude of the current decreased below a threshold set to five standard deviations from the open channel mean conductance for at least $420 \mu\text{s}$ (figure 3). In previous reports, events as short as $40 \mu\text{s}$ were analyzed. Including short events in the data reduction allows for more extensive analysis of the event kinetics at the expense of improved signal-to-noise achieved through the averaging techniques described in detail elsewhere and briefly below.

The time for the start, t_{on} , and end, t_{off} , of the blockade are estimated as the times at which the current crosses the threshold. With the duration defined, the open state of the pore is determined by a simple averaging technique described with the following expression,

$$\langle i_o \rangle = \frac{1}{80} \sum_{k=1}^{40} i(t_{\text{on}} - (k+9)t_s) + i(t_{\text{off}} + (k+9)t_s) \quad (1)$$

where $\langle i_o \rangle$ is the time averaged open state current (the gray shaded area in figure 3), $i(t)$ is the time-dependent current and t_s is the sampling time ($20 \mu\text{s}$). The rise time of a typical electrophysiology amplifier was analyzed by Uram and Mayer [21]. Neglecting some of the finer details of their analysis, the step function response of the digital filter used here initiates ringing and other deleterious filter effects [22],

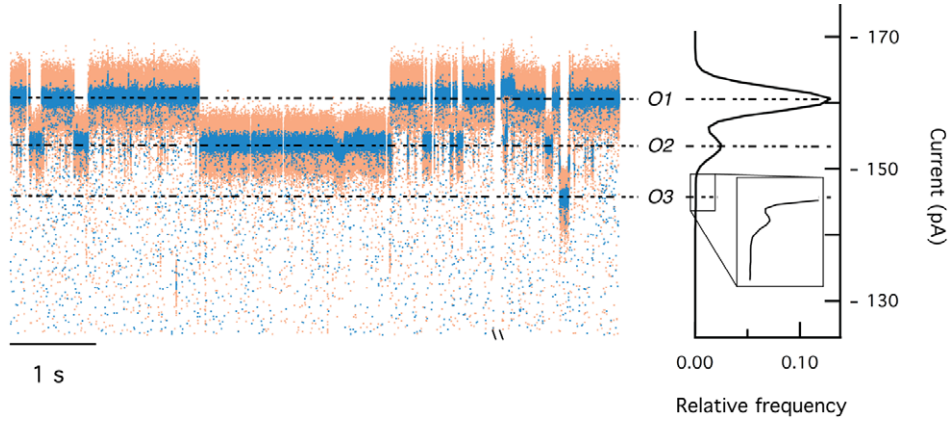


Figure 2. An expanded view of the open channel shows the channel switch between at least three stable open states $O1$, $O2$, and $O3$, filtered at 10 kHz (orange) and 1 kHz (blue). The stray points below ~ -145 pA are transitions to the polymer-induced blockades not shown in this plot. The relative frequency of each state can be observed directly in an all-points histogram of the time series trace (right). It should be noted that the data shown is selected to show clear examples of each state. From the histogram, $O3$ is exceedingly rare and will only be observed with sufficiently long data sets.

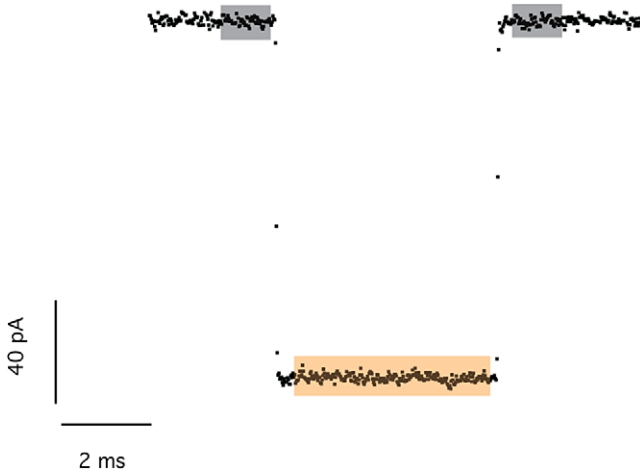


Figure 3. A simple thresholding algorithm detects single blockade events. The blockade amplitude is defined by averaging the open channel current immediately adjacent to the event, $\langle i_o \rangle$ (gray shaded region), and the base of the blockade, $\langle i \rangle$ (orange shaded region).

which we avoid by calculating the open state average from 40 data points 10 points before and 10 points after the current crosses the threshold (see figure 3). In addition to smoothing the filter effect, this imposed condition guarantees that the open state does not change during a blockade. A relative distribution of the tabulated open state currents between -145 and -170 pA was created with a 200-bin histogram of the calculated open states from >10000 blockade events (figure 4). This histogram is dominated by two broad peaks, which correspond to $O1$ and $O2$. Close inspection of $O1$ and $O2$ indicates that each of these peaks is composed of at least three open current states, which we fit with a Gaussian mixture. The peak position of each of these sub-peaks is $O1_1 = -162.5$ pA, $O1_2 = -161.2$ pA and $O1_3 = -160.0$ pA and $O2_1 = -155.2$ pA, $O2_2 = -154.1$ pA and $O2_3 = -153.2$ pA. These states have only been examined in the presence of PEG. The physical source and control of these states is the subject of future investigations.

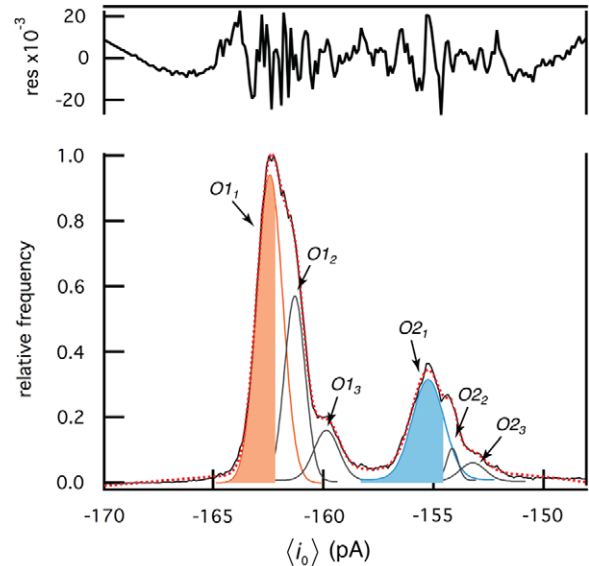


Figure 4. The open channel histogram, $\langle i_o \rangle$, resolves a triplet of states for each of the major conductance bands seen in figure 2. Gaussian distributions were fit to the data to estimate the probability density of each state. The Gaussian distributions shown in orange, blue and gray are added to produce an overall distribution (red, dashed), which is compared to the data (black, solid). The residual of the fit is displayed above. The events that fall within the orange and blue regions have less than 1% overlap with other opens states and were used for further analysis herein.

An analysis of the polymer-induced blockades was done in a similar fashion to the open state detection. The average current of each blockade event was calculated by averaging a limited range of the blockade current (see data highlighted in orange in figure 3) with the expression,

$$\langle i \rangle = \frac{1}{k_{\max}} \sum_{k=1}^{k_{\max}} i(t_{\text{on}} + (k + 10)t_s) \quad (2)$$

where $k_{\max} = ((t_{\text{off}} - t_{\text{on}})/t_s) - 18$ was chosen to eliminate errors associated with bandwidth-related oscillations [22].

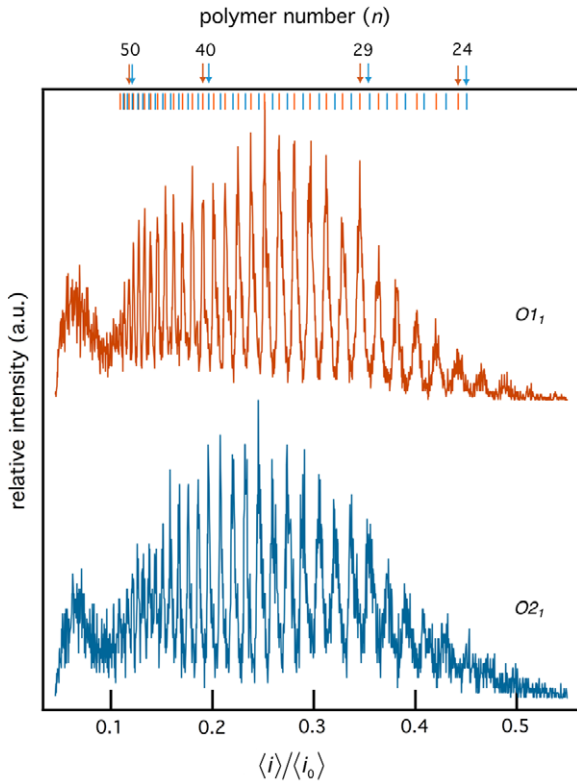


Figure 5. PEG-induced single channel current reduction distributions show open state dependent peak positions. The high current open state shows a greater degree of blockade (orange) than the lower current open state (blue). The color-coded tick marks correspond to the peak positions and show the offset in $\langle i \rangle / \langle i_0 \rangle$ between the two open states O_{1_1} and O_{2_1} . The solution contained a mixture of PEGs with approximately equimolar concentrations of mean molecular masses $M_w = 1000, 1500, 2000$ and 3000 g mol^{-1} and a chemically purified standard of PEG $M_w = 1294 \text{ g mol}^{-1}$ ($n = 29$), resulting in a broad distribution of resolvable polymers ranging from $n = 24$ to $n > 55$.

Once the $\langle i \rangle / \langle i_0 \rangle$ values for each event are tabulated, separate histograms with 2000 bins are constructed for open states O_{1_1} and O_{2_1} . The distribution is further refined by rejecting events with a greater than 1% probability of belonging to neighboring sub-peaks (see shaded regions in figure 4). For each open state, a series of peaks analogous to a mass spectrogram is observed [10] (figure 5). By using the internal standard at $n = 29$, the mass distribution for each dataset can be directly determined. The most striking difference between the two datasets is the slight shift in the peak positions, which is plotted directly in figure 6.

3. Origin of the open state transitions

The variation in the open channel conductance could be caused by either metastable nanoscale leaks in the membrane or different geometric configurations of the nanopore. We consider here the effect these phenomenon would separately have on the ratio of the blockade peak positions and show in the results section that our data support the latter mechanism.

If we assume the different open state currents, parameterized by j , originate from a leaky membrane, then the measured

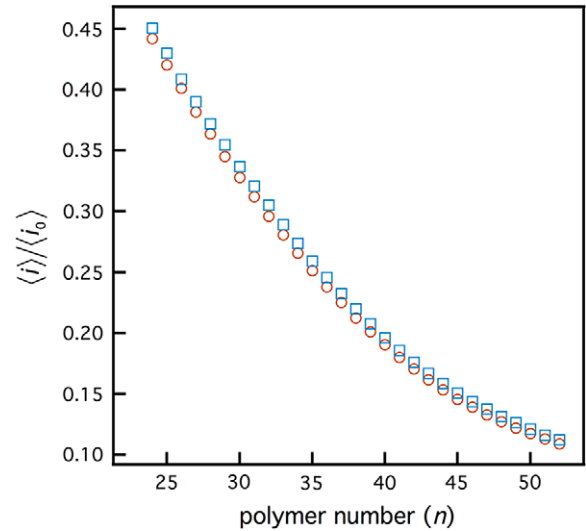


Figure 6. The relative current blockades for the open states O_{1_1} (orange circles) and O_{2_1} (blue squares) show a quasi-exponential dependence on the polymer number with the shift in peak positions.

current blockade ratio for each open state r_j can be written as

$$r_j \equiv \frac{\langle i \rangle_{j,m}}{\langle i_0 \rangle_{j,m}} = \frac{\langle i \rangle_t + \langle i_{\text{leak},j} \rangle}{\langle i_0 \rangle_t + \langle i_{\text{leak},j} \rangle} \quad (3)$$

where the m subscript refers to the measured value, the t subscript refers to the true or nanopore only current values, and $\langle i_{\text{leak},j} \rangle$ is the leakage current of the j th open state. The ratio of measured blockade depths for open states O_{1_1} and O_{2_1} depends on the relative difference of the open state currents $\delta = (\langle i_0 \rangle_{O_{1_1},m} - \langle i_0 \rangle_{O_{2_1},m}) / \langle i_0 \rangle_{O_{2_1},m}$ and the measured current blockades for the second open state $r_{O_{2_1}}$

$$r \equiv \frac{r_{O_{2_1}}}{r_{O_{1_1}}} = \frac{1 + \delta}{(1 + \delta/r_{O_{2_1}})} \quad (4)$$

Figure 7 shows explicitly the data presented as $r - 1$ (open circles). If well-defined and persistent leakage currents are responsible for the observed peak shifts, then equation (4), with no free parameters, should fit the data. However, the calculated ratio not only has the wrong sign (i.e., $r_{O_{2_1}} < r_{O_{1_1}}$), but it is also ~ 1 order of magnitude too large (data not shown). Because equation (4) diverges so drastically from the measured current blockade ratios, well-defined and persistent leakage currents in the membrane cannot cause the different open states.

We now consider whether the changes in the open state current are the result of shifts in the nanopore geometry. In its native conformation, the sensing region of the α HL channel is a 49.5 \AA long β -barrel with a cross-sectional area of 450 \AA^2 [23]. Metastable states might correspond to different conformations of pore with different cross-sectional areas and lengths. If that were the case, one would expect that the open state currents and peak positions in the normalized current blockade distribution would depend on the pore geometry. Several different open state configurations were observed and simulated previously. Some examples include

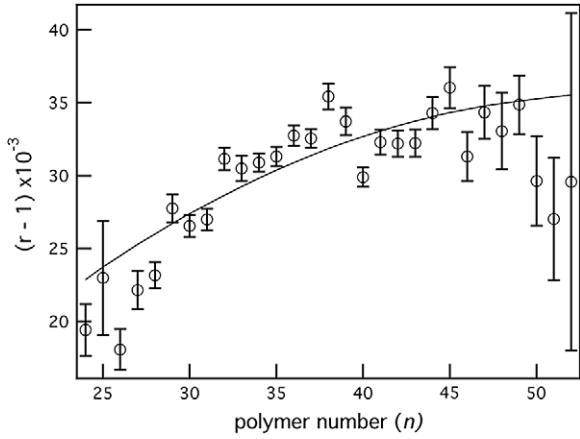


Figure 7. Test of two mechanisms for the open channel conductance changes. The ratio of peak positions ($\frac{r_{O2_1}}{r_{O1_1}} - 1$) were calculated from the measured peak positions in figure 6 (open circles). The solid line is a single parameter fit of the pore geometry change model (equation (9)). The shift in the peak position ratio is more accurately described by changes in the nanopore geometry than by leakage currents.

a pore formed from proteolytically nicked monomers [24] or a hexameric pore [25–27], where both show conductance values of approximately half the heptameric nanopore. Although there are different conductance states of the ‘fully open’ α HL channel, they were likely ignored due to low signal-to-noise values [10, 20]. Here, we combine the observed difference in the open state currents with the apparent shift in the peak position distributions of PEG-induced blockades to approximate changes in both the axial length L_{pore} and cross-sectional area A_{pore} of the nanopore.

The relative current blockade for PEG in a right-circular cylinder is modeled here by assuming the PEG molecule with average length L_{PEG} along the axial coordinate of the nanopore and average cross-sectional area A_{PEG} partially blocks the flow of ions [10, 28]. As in [16] we assume the density of the confined PEG is equal to 1.09 g cm^{-3} and that L_{PEG} grows along the nanopore in a manner analogous to a polymer in a good solvent so that $L_{\text{PEG}} = an^\nu$ where $a = 1.45 \text{ \AA}$ so that $A_{\text{PEG}} = bn^{1-\nu}$. We assume that $b = 46.5 \text{ \AA}^2$ and $\nu = 0.6$ [16]. A more detailed model of how PEG occupies the nanopore is beyond the scope of this work and is the subject of future study. For now, we assume the PEG occupied nanopore can be modeled as two resistors in series so that the ratio of the current between the PEG occupied nanopore and the open state nanopore is given by

$$\frac{\langle i \rangle_t}{\langle i_o \rangle_t} = \frac{R_{\text{open}}}{R_{\text{PEG}} + R_{\text{open}}^{\text{PEG}}} \quad (5)$$

where $R_{\text{open}} = \rho_o L_{\text{pore}} / A_{\text{pore}}$ is the electrical resistance of the PEG-free nanopore with resistivity ρ_o , $R_{\text{PEG}} = \rho_{\text{PEG}} L_{\text{PEG}} / (A_{\text{pore}} - A_{\text{PEG}})$ is the resistance of the PEG occupied region of the nanopore with resistivity ρ_{PEG} and $R_{\text{open}}^{\text{PEG}} = \rho_o (L_{\text{pore}} - L_{\text{PEG}}) / A_{\text{pore}}$ is the resistance of the PEG-free region of the polymer-occupied nanopore. Substituting these terms into equation (5) leads to the following expression

for the magnitude of the open state normalized current blockades

$$\frac{\langle i \rangle_t}{\langle i_o \rangle_t} = \frac{1}{1 - z} \quad (6)$$

where z is

$$z = \frac{L_{\text{PEG}}}{L_{\text{pore}}} \left(1 - \frac{\rho_{\text{PEG}} / \rho_o}{1 - A_{\text{PEG}} / A_{\text{pore}}} \right). \quad (7)$$

$\rho_{\text{PEG}} / \rho_o$ depends in a non-trivial way on the size of the PEG molecule and we have used a first-order binding model to estimate it elsewhere [16]. For the purpose of this manuscript, we only estimate the changes in L_{pore} and A_{pore} that correspond to the different open states. For simplicity, we assume that $\rho_{\text{PEG}} / \rho_o$ is independent of L_{pore} and A_{pore} . The ratio of the two open state currents is

$$r_{\text{open}} \equiv \frac{\langle i_o \rangle_{O1_1}}{\langle i_o \rangle_{O2_1}} = \frac{1 + \delta L_{\text{pore}}}{1 + \delta A_{\text{pore}}} \quad (8)$$

where $\delta x = \frac{x_{O2_1} - x_{O1_1}}{x_{O1_1}}$ and we have assumed the resistivity of the nanopore is the same for both open state conformations. When the open state currents differ by only a few per cent, the ratio of the PEG-induced current blockades for the two open states (equation (4)) can be estimated to first order in δA_{pore} and δL_{pore}

$$r \approx 1 + \alpha(\delta L_{\text{pore}}) + \beta \left(\alpha + r_{O1_1} \frac{L_{\text{PEG}}}{L_{\text{pore}|O1_1}} \right) (\delta A_{\text{pore}}) \quad (9)$$

where $\alpha = 1 - r_{O1_1}$, and $\beta = \left(\frac{A_{\text{pore}|O1_1}}{A_{\text{PEG}}} - 1 \right)^{-1}$. Equation (8) fixes ΔA_{pore} with respect to ΔL_{pore} and a least squares fit of equation (8) (with one free independent parameter) to the measured ratio of PEG-induced blockades for both open states provides an estimate of ΔL_{pore} (solid line, figure 7). The fit of the data with equation (9) results in an estimated ΔL_{pore} of $(4.23 \pm 0.04)\%$ and ΔA_{pore} of $(-0.39 \pm 0.04)\%$ (reduced $\chi^2 = 4.6$; weighed by the propagated standard error). This is a remarkably good fit for a one-parameter model. Further improvements could use a more complicated pore geometry [23], include fixed charges inside the nanopore structure [29] and model the dependence of $\rho_{\text{PEG}} / \rho_o$ on the pore geometry [16]. If the length of the nanopore in the high current open state is 49.5 \AA , then the length in the low current open state should be 51.7 \AA (a net change of 2.2 \AA) while the cross-sectional area decreases from 450 to 449 \AA^2 corresponding to a change in diameter of $<0.1 \text{ \AA}$. Because the underside of the cap domain of the protein is in intimate contact with lipid headgroups as suggested by the crystal structure [23] and further confirmed by neutron reflectometry for the channel in a biomimetic membrane [30], it is conceivable that the channel reversibly switches between these states because it encounters regions in the membrane that contain varying amounts of solvent, different thickness or different local stiffness.

4. Summary and conclusion

Although different open states of the α HL nanopore were noted more than 15 years ago, they have been ignored in

nanopore-based sensing of analytes. The results above suggest that if the open state is not rigorously controlled, analyte misidentification will occur. This is an important issue for all applications of nanopore analysis including polymer analysis, DNA sequencing and protein characterization.

In this work, the cause of shifts in the channel open state was determined and the results will improve the analytical capabilities of the α HL nanopore. Moreover, because each open state produces unique molecular spectra, the peak shifts can be used to further refine the radius of the nanopore to radial differences on the order of 2–3 covalent bonds. Finally, resolving the PEG- α HL interactions to the single monomer limit dramatically improves the established PEG nanopore sizing technique. Here, we suggested a new technique that could study dynamic changes of membrane-bound nanopores. In combination with other existing structural techniques, our method could lead to a more complete structure-function description of a membrane-bound nanopore.

Acknowledgments

We thank Electronic Biosciences, LLC for building a high-impedance amplifier and data acquisition system for our laboratory under a NIST SBIR grant. Henry White provided helpful instructions for working with conical glass pores as membrane supports and generously donated glass nanopore supports. This work was sponsored in part by grants from the NIST Office of Microelectronics Program and the NIST Office of Law Enforcement Standards. Certain commercial equipment, instruments, or materials are identified in this work to specify the experimental procedure adequately. Such identification is not intended to imply recommendation or endorsement by the National Institute of Standards and Technology, nor is it intended to imply that the materials or equipment identified are necessarily the best available for this purpose.

References

- [1] Coulter W H 1953 *US Patent Specification* 2,656,508
- [2] Deblois R W and Bean C P 1970 *Rev. Sci. Instrum.* **41** 909
- [3] Bezrukov S M and Kasianowicz J J 1993 *Phys. Rev. Lett.* **70** 2352
- [4] Kasianowicz J J, Brandin E, Branton D and Deamer D W 1996 *Proc. Natl Acad. Sci. USA* **93** 13770
- [5] Kasianowicz J J, Robertson J W F, Chan E R, Reiner J E and Stanford V M 2008 *Annu. Rev. Anal. Chem.* **1** 737
- [6] Bohn P W 2009 *Annu. Rev. Anal. Chem.* **2** 279
- [7] Howorka S and Siwy Z 2009 *Chem. Soc. Rev.* **38** 2360
- [8] Piruska A, Gong M, Sweedler J V and Bohn P W 2010 *Chem. Soc. Rev.* **39** 1060
- [9] Siwy Z S and Howorka S 2010 *Chem. Soc. Rev.* **39** 1115
- [10] Robertson J W F, Rodrigues C G, Stanford V, Rubinson K A, Krasilnikov O V and Kasianowicz J J 2007 *Proc. Natl Acad. Sci. USA* **104** 8207
- [11] Zimmerberg J and Parsegian V 1986 *Nature* **323** 36
- [12] Krasilnikov O, Sabirov R, Ternovsky V, Merzliak P and Muratkhodjaev J 1992 *FEMS Microbiol. Immun.* **105** 93
- [13] Merzlyak P G, Yuldasheva L N, Rodrigues C G, Carneiro C, Krasilnikov O V and Bezrukov S M 1999 *Biophys. J.* **77** 3023
- [14] Krasilnikov O V 2002 *Sizing channels with neutral polymers Structure and Dynamics of Confined Polymers* ed J J Kasianowicz, M S Z Kellermayer and D W Deamer (Dordrecht: Kluwer)
- [15] Nablo B J, Halverson K M, Robertson J W F, Nguyen T L, Panchal R G, Gussio R, Bavari S, Krasilnikov O V and Kasianowicz J J 2008 *Biophys. J.* **95** 1157
- [16] Reiner J E, Kasianowicz J J, Nablo B J and Robertson J W F 2010 *Proc. Natl Acad. Sci. USA* **107** 12080
- [17] Ervin E N, White R J and White H S 2009 *Anal. Chem.* **81** 533
- [18] White R J, Ervin E N, Yang T, Chen X, Daniel S, Cremer P S and White H S 2007 *J. Am. Chem. Soc.* **129** 11766
- [19] White R J, Zhang B, Daniel S, Tang J M, Ervin E N, Cremer P S and White H S 2006 *Langmuir* **22** 10777
- [20] Kasianowicz J J and Bezrukov S M 1995 *Biophys. J.* **69** 94
- [21] Uram J D, Ke K and Mayer M 2008 *ACS Nano* **2** 857
- [22] Horowitz P and Hill W 1989 *The Art of Electronics* 2nd edn (Cambridge: Cambridge University Press)
- [23] Song L Z, Hobaugh M R, Shustak C, Cheley S, Bayley H and Gouaux J E 1996 *Science* **274** 1859
- [24] Krasilnikov O V, Merzlyak P G, Yuldasheva L N, Azimova R and Nogueira R 1997 *Med. Microbiol. Immun.* **186** 53
- [25] Czajkowsky D M, Sheng S and Shao Z 1998 *J. Mol. Biol.* **276** 325
- [26] Furini S, Domene C, Rossi M, Tartagni M and Cavalcanti S 2008 *Biophys. J.* **95** 2265
- [27] Kawate T and Gouaux E 2003 *Protein Sci.* **12** 997
- [28] Krasilnikov O V, Rodrigues C G and Bezrukov S M 2006 *Phys. Rev. Lett.* **97** 018301
- [29] Aksimentiev A and Schulten K 2005 *Biophys. J.* **88** 3745
- [30] McGillivray D J, Valincius G, Heinrich F, Robertson J W F, Vanderah D J, Febo-Ayala W, Ignatjev I, Losche M and Kasianowicz J J 2009 *Biophys. J.* **96** 1547